A Dual-Function Highly Crystalline Covalent Organic Framework for HCl Sensing and Visible-light Heterogeneous Photocatalysis

Yogendra Nailwal[†], A. D. Dinga Wonanke[‡], Matthew A. Addicoat[‡] and Santanu Kumar Pal*[†]

[†]Department of Chemical Sciences, Indian Institute of Science Education and Research (IISER) Mohali, Sector 81, Knowledge City, Manauli, 140306 (India), E-mail: skpal@iisermohali.ac.in, santanupal.20@gmail.com

[‡]School of Science and Technology, Nottingham Trent University, Clifton Lane, NG11 8NS, Nottingham, United Kingdom

Truxene-based COFs, COFs as HCl Sensor, Photocatalysis, High stability, Porous polymers

ABSTRACT: Covalent organic frameworks (COFs) offer great potential for various advanced applications such as photocatalysis, sensing, etc., because of their fully conjugated, porous, and chemically stable unique structural architecture. In this work, we have designed and developed a truxene based ultrastable COF (Tx-COF-2) by Schiff-base condensation between 1,3,5-Tris(4-aminophenyl)benzene (TAPB) and 5,5,10,10,15,15-hexamethyl-10,15-dihydro-5H-diindeno(1,2-a:1',2'-c)fluorene-2,7,12-tricarbaldehyde (Tx-CHO) for the first time. The resulting COF possesses excellent crystallinity, permanent porosity, and high Brunauer–Emmett–Teller (BET) surface areas (up to 1137 m^2g^{-1}). The COF was found to be a heterogeneous, recyclable photocatalyst for efficient conversion of arylboronic acids to phenols under visible-light irradiation, an environmentally friendly alternative approach to conventional metal-based photocatalysis. Besides, Tx-COF-2 provides an immediate naked-eye color change (<1s) and fluorescence 'turn-on' phenomena upon exposure to HCl. The response is highly sensitive, with an ultra-low detection limit of up to 4.5 nmol L^{-1}.

Covalent organic frameworks (COFs) are the emerging class of porous organic materials, constructed from various building blocks, connected via strong covalent organic bonds.[1] In recent years, COFs have gained immense interest due to their extraordinary properties such as low density, high porosity, extreme crystallinity, and their capability of introducing new organic moiety inside the stable framework.[2] Due to these properties, COFs have expanded their dimensions into various applications such as gas storage and separation,[3] sensing,[4] energy storage and conversion,[5] proton conduction,[6] optics,[7] catalysis,[8] and so on. In terms of photocatalysis, they have received enormous attention from the past decade because of the combination of their π-conjugated framework, regular pore structure, tunable pore channels, high surface area, and most importantly, their insolubility in all organic solvents, which is the key feature for their heterogeneous character. These features demonstrate that COFs could be considered as a potential candidate for photocatalytic applications.

Among several π-conjugated molecules used as a monomer for the construction of COFs, our particular interest is in the heptacyclic truxene unit. Truxene can be considered as 1,3,5-triphenylbenzene clipped through three bridging methylene groups in a plane. These three methylene groups aid planarization of the system and extend the π-conjugation by forming three additional fused five-membered rings.[9] This unique structural motif provides truxene to be an attractive photoactive core and enhances electron-donating capabilities.[10] The flat trigonal geometry of the truxene has raised interest as a monomer in the construction of functional conjugated microporous polymers (CMPs) and COFs for various applications.[11] Herein, for the first time, we have designed and synthesized a truxene based [3+ 3] COF using Schiff's-based chemistry and demonstrated its dual function both as a heterogeneous photocatalyst and a naked-eye acid sensor.

Recently, photocatalysis has become a vital category in organic synthesis due to its mild reaction conditions such as room temperature and atmospheric pressure, simple setup, and most importantly, environmentally friendly alternative to the metal-based catalysts.[12] However, inorganic transition metal-complexes[13] and organic dyes[14] have already shown various chemical transformations as homogeneous photocatalysts. These metal-based photocatalysts and organic dyes are commercially available, and they possess excellent stability. However, their intrinsic drawbacks,

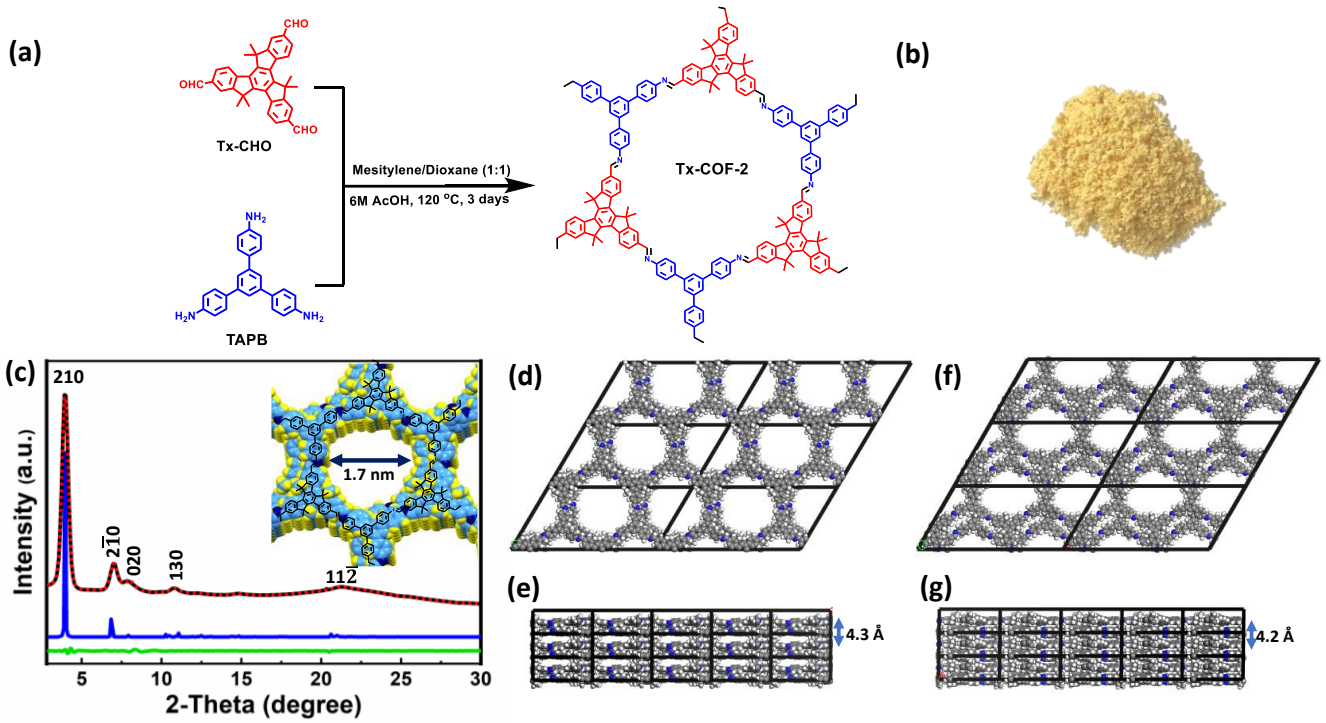

Figure 1. (a) Schematic representation of Tx-COF-2 synthesis. (b) The physical appearance of Tx-COF-2. (c) PXRD patterns of Tx-COF-2: experimental (black) and Pawley refined (red, dotted), simulated PXRD pattern of slipped AA mode (blue), and difference plot (green) between the refined and experimental PXRD patterns. (d, e) Top view and side view of the slipped AA stacking mode of Tx-COF-2 and (f, g) Top view and side view of staggered AB stacking mode of Tx-COF-2.

postreaction removal cost of homogeneous catalysts, etc., limit their widespread use in large-scale synthesis used for commercial applications. Therefore, the demand for metal-free, heterogeneous catalysts with high stability, easy recovery, and reusability from the reaction mixture could reduce the aforementioned concerns.

In this article, we report the synthesis of Tx-COF-2 (Figure 1a) by performing a reaction between 1,3,5-Tris(4-aminophenyl)benzene (TAPB) and 5,5,10,10,15,15-hexamethyl-10,15-dihydro-5H-diindeno(1,2-a:1',2'-c)fluorene-2,7,12 tricarbaldehyde (Tx-CHO). The reaction was carried out under solvothermal conditions and heated at 120 °C for three days by employing a solvent combination of Mesitylene/Dioxane (1:1, v/v) and 6 M acetic acid as a catalyst. Interestingly, Tx-COF-2 exhibited high BET surface areas up to 1137 m^2g^{-1}, extraordinary stability in harsh chemical conditions such as 12 M NaOH, 12 M HCl, and irradiation of visible light for minimum 5 days. Tx-COF-2 showed excellent photocatalytic performance for the aerobic oxidative hydroxylation of arylboronic acids. It retained its crystallinity and activity even after the 10^{th} photocatalytic cycle. Moreover, Tx-COF-2 was shown to be a selective 'switch-on' sensor for HCl. Upon exposure to HCl, it became fluorescent and reverted to its negligible fluorescent intensity (pristine) after exposure to NH_3 vapor. Most importantly, a naked-eye reversible color change from light yellow to orange was also observed when treated alternatively with HCl and NH_3 vapor both in solid and in the dispersed medium of Tx-COF-2.

In a typical synthesis, Tx-COF-2 was synthesized by the Schiff-base condensation reaction between 1,3,5 Tris(4-aminophenyl) benzene (TAPB), (27.5 mg, 0.078 mmol), 5,5,10,10,15,15-hexamethyl-10,15-dihydro-5H-diindeno(1,2-a:1',2'-c)fluorene-2,7,12-tricarbaldehyde (Tx-CHO, Figure S1, S2), (40 mg, 0.078 mmol) and 0.5 mL of 6 M aqueous acetic acid, heated in a Schlenk tube for 72 hours under solvothermal condition (Figure 1a). The solvothermal conditions were screened with various solvent combinations, and the best crystallinity was obtained in Mesitylene/Dioxane (1:1 by volume) solvent mixture (Figure S4). To characterize the successful formation of Tx-COF-2, we first employed Fourier transform infrared (FT-IR) spectroscopy. As shown in the FT-IR spectra of Tx-COF-2 (Figure S3), the stretching band of C=O at 1695 cm^{-1} in Tx-CHO and stretching bands of amine (N-H, ~3437 cm^{-1}, 3357 cm^{-1}) in TAPB disappeared. The appearance of a new vibrational band nearly at 1624 cm^{-1} indicated the formation of an imine bond (C=N) in Tx-COF-2, which is consistent with prior studies.[15] Furthermore, solid-state ^{13}C cross-polarization - magic angle spinning nuclear magnetic resonance (CP-MAS NMR) spectroscopy of Tx-COF-2 revealed peaks at 22 and 46 ppm, which originated from the methyl groups and tertiary carbon of the truxene unit, respectively. The other signals in the range of 120−150 ppm can be assigned to the aromatic carbons present in the framework. Further, a signal at 157.9 ppm is indicative of the existence of imine linkage in Tx-COF-2 (Figure 2a) which supports the formation of the reticular framework.

The crystalline structure of Tx-COF-2 was confirmed by powder X-ray diffraction (PXRD) analysis with Cu Kα radiation. As shown in Figure 1c, the PXRD pattern of Tx-COF-2 showed high crystallinity, with the first intense peak at a low 2Θ value of 3.93°, which corresponds to (210) reflection

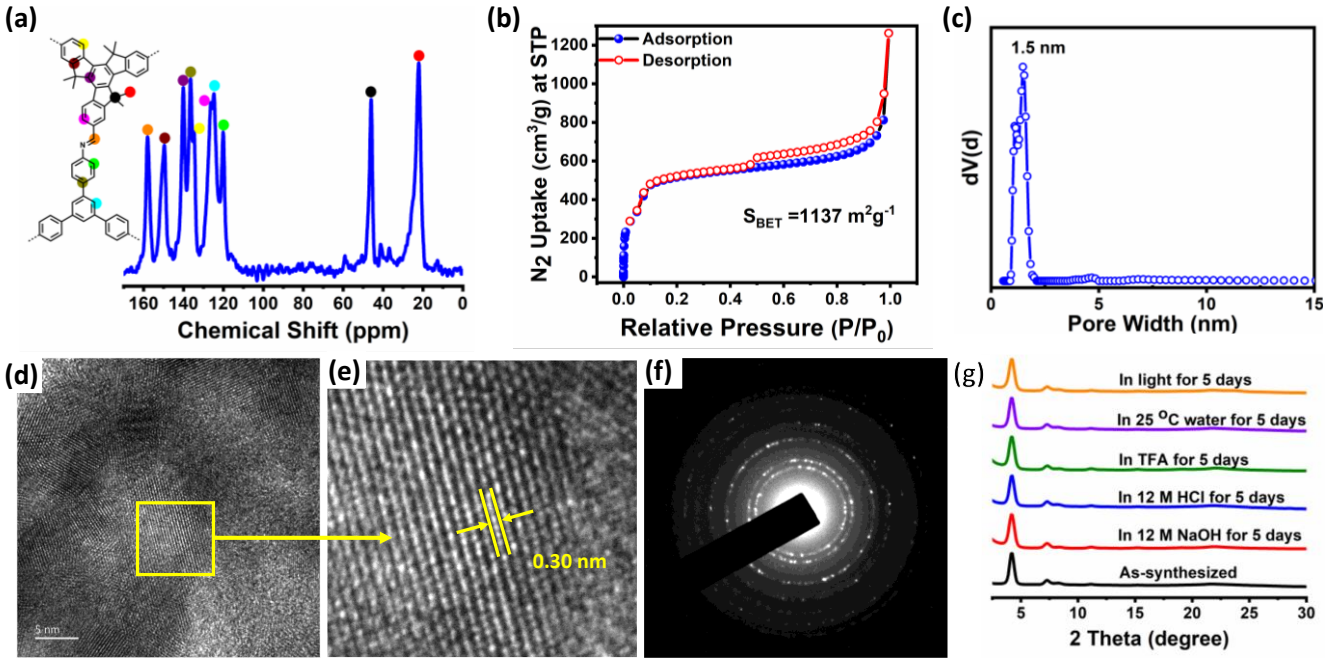

Figure 2. (a) Solid-state ^{13}C NMR spectrum of Tx-COF-2. (b) Nitrogen adsorption and desorption isotherms of Tx-COF-2. (c) The pore size distribution (PSD) was calculated from the QSDFT method of Tx-COF-2. (d) HRTEM image of Tx-COF-2. (e) Zoomed HRTEM image of the marked yellow area in (d), showing the interlayer stacking distance of 0.30 nm. (f) SAED patterns Tx-COF-2 showing the presence of various crystalline phases and (g) PXRD profiles of Tx-COF-2 pristine (black) and after treating with visible light (orange), 12 M HCl (blue), TFA (green), 12 M NaOH (red), and water (purple) for 5 days.

plane, along with minor peaks at 7.20°, 8.20°, 11.0°, 21.21° corresponding to the $(2\bar{1}0)$, (020), (130), and $(11\bar{2})$ facets, respectively. In order to elucidate the structure of Tx-COF-2 and to calculate the unit cell parameters, a monolayer of Tx-COF-2 (hcb net) was built, and several stacking configurations were generated including, eclipsed (AA), slipped stacking (slipAA), and staggered stacking (AB) models (Figure 1). These structural models were optimized by density-functional tight-binding (DFTB) calculations as implemented in DFTB+ 19.1. The comparison between the simulated PXRD pattern and experimental PXRD data indicated that the experimental PXRD profile matched well to the simulated pattern with slipped AA stacking in the triclinic system, P1 space group (Figure 1c, Figure S5). Additionally, the lower value of the stacking energy of the model with slipped AA stacking (-355.1 kJ/mol) than that of AB stacking (-256.7 kJ/mol) further supported that Tx-COF-2 adopted slipped AA stacking. The obtained powder pattern was refined by Pawley refinement which gave a unit cell with parameters as follows: a = 51.7 Å, b = 25.8 Å, c = 8.6 Å, α =90.0°, β = 91.3°, γ = 59.2°. The final R_{wp} and R_p values converged to 0.59% and 0.33%, respectively.

The permanent porosity of Tx-COF-2 was evaluated by the nitrogen adsorption-desorption experiment, measured at 77 K. As shown in Figure 2b, Tx-COF-2 displayed a typical type I reversible isotherm, indicating a microporous nature. The BET surface area was calculated to be 1137 m^2g^{-1} (Figure S6). Furthermore, the quenched solid density functional theory (QSDFT) method was applied to calculate the pore size distribution (PSD). The method suggested a narrow pore size distribution with a prominent peak at 1.51 nm, which is in good agreement with the pore size calculated (1.7 nm, Figure 1c) from the simulated model (Figure 2c). The morphologies of the Tx-COF-2 were studied by electron microscopy. A particulate morphology was revealed by Field Emission Scanning Electron Microscopy (FE-SEM) of Tx-COF-2 (Figure S7). Further, the finer detail of the internal structure of Tx-COF-2 was revealed by HRTEM analysis. HRTEM showed an ordered, hexagonal porous structure, which was in accordance with the structural model. We observed well-defined lattice fringes of 0.30 nm (Figure 2d, 2e), corroborating with the interlayer stacking distance obtained from PXRD analysis (0.42 nm) and from slipAA simulated model (0.43 nm) analysis. Furthermore, the SAED pattern revealed various highly crystalline phases present in the Tx-COF-2 (Figure 2f).

Tx-COF-2 showed excellent thermal as well as chemical stability. The thermogravimetric analysis suggested that Tx-COF-2 was stable up to 375 °C under the nitrogen atmosphere (Figure S8). PXRD assessed the chemical stability of the COF after 5 days of treatment in water, TFA, 12 M HCl, 12 M NaOH. In all these harsh conditions, Tx-COF-2 retained its crystallinity. Furthermore, most of the reported imine-linked COFs degraded upon irradiation of light for a long time,[16] Tx-COF-2 showed no degradation in the crystallinity after irradiation with 20 W white-light-emitting diodes (WLED) for 5 days (Figure 2g). The high stability towards harsh chemicals and photostability of Tx-COF-2 render it an excellent candidate for heterogeneous photocatalysis.

The extensively conjugated structure, high chemical stability and photostability of Tx-COF-2 led us to think whether it could act as a metal-free heterogeneous photocatalyst. We chose visible-light-induced oxidative hydroxylation of arylboronic acids to phenols to test its photoactivity since metal-free heterogeneous photocatalysis provides an environmentally friendly alternative to the traditional metal-based redox-chemical processes. Additionally, phenols are well-known, versatile intermediates and building blocks in natural products, polymers, and pharmaceutical industries.[17] In previous reports, it was illustrated that

oxidative hydroxylation of arylboronic acids to produce phenols could be done by using homogeneous photoredox catalysts, such as Ir or Ru complexes[18] and methylene blue (MB).[19] Ruthenium and Iridium complexes, such as $Ru(bpy)_3Cl_2$ and $Ir(PPy)_3$ are most commonly used for visible light photocatalysts.[20] $Ru(bpy)_3Cl_2$ and similar complexes also have been used for the water splitting[21] and the reduction of CO_2 to methane, [22] OLEDs,[23] and initiator for polymerization reactions[24] or in photodynamic therapy.[25] $Ru(bpy)_3Cl_2$ has also been used as visible light photoredox catalyst for α-alkylation of aldehydes,[26] [2 + 2] cycloaddition[27] and reductive dehalogenation of activated alkyl halides.[28] Compared to these earlier works, our COF is designed to provide a heterogeneous catalytic environment so that reusability and recyclability of the photocatalyst can be achieved easily.

Table 1. Control Experiments[a]

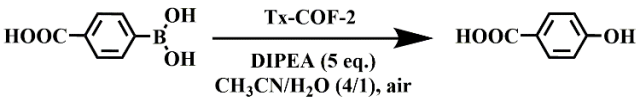

Entry	Visible Light	Photocatalysts	Atmosphere	Additives	Yield[b](%)
1	ON	Tx-COF-2	Air	-	99
2	ON	Tx-COF-2	O_2	-	99
3	ON	Tx-COF-2	N_2	-	N.D.[c]
4	OFF	Tx-COF-2	Air	-	N.D.[c]
5	ON	No catalyst	Air	-	N.D.[c]

[a]Conditions: 4-Carboxyphenylboronic Acid (0.12 mmol), Tx-COF-2 (10 mg, 0.012 mmol), CH_3CN (1.6 mL), H_2O (0.4 mL), DIPEA (5.0 eq.), irradiation with 20 W white LEDs, 48 h. [b]Yields of isolated products. [c]N.D. = not detected.

In the recent past, a couple of COFs containing benzoxazole core[16] and vinylene-bridged COFs[29] have already shown photocatalytic activity for the conversion of boronic acids to phenols. We believe that in our work, the photocatalytic activity of Tx-COF-2 could be a result of the highly electron-rich truxene (Tx-CHO) unit.[30] Thus, we selected the conversion of 4-carboxyphenylboronic acid to 4-hydroxybenzoic acid as a model reaction for the systematic evaluation of the reaction. The elements which influence this transformation, such as photocatalyst, light source, oxygen source, and sacrificial agent, were evaluated systematically. As shown in Table 1, yield of the reaction can be obtained up to 99% with *N*,*N*-diisopropylethylamine (DIPEA) as a sacrificial agent and Tx-COF-2 as a photocatalyst under air or oxygen atmosphere in the presence of visible light. In the absence of Tx-COF-2, no conversion was observed (Table 1, entry 5), which suggested that Tx-COF-2 has a significant part as a photocatalyst. Similarly, the transformation of the reaction was hard to observe when conducted in the absence of light and in N_2 atmosphere (Table 1, entries 3 and 4). It could be concluded from all these control experiments that light source, oxygen, and photocatalyst are necessary for this reaction.

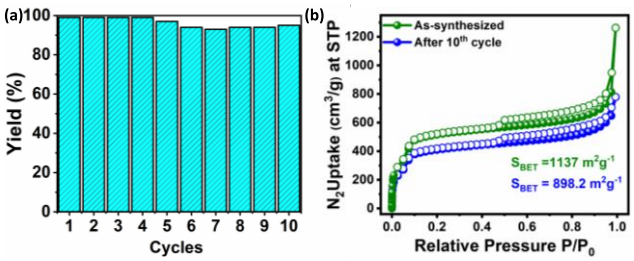

Figure 3. (a) Reusability of Tx-COF-2 for oxidative hydroxylation of 4-carboxyphenylboronic acid and (b) N_2 adsorption isotherm of Tx-COF-2 before (olive) and after (blue) 10th catalytic cycle.

The superiority of Tx-COF-2 as a photocatalyst was further examined by recycling experiments. Because of the insoluble nature of Tx-COF-2 in all common organic solvents, it can be simply separated by centrifugation from the reaction. The experiment was performed on 4-carboxyphenylboronic acid. As shown in Figure 3a, without any reactivation procedure or specific treatment, the conversion efficiency of 4-carboxyphenylboronic acid to 4-hydroxybenzoic acid Tx-COF-2 gave excellent conversion even after 10 runs as a photocatalyst. The crystallinity of recycled Tx-COF-2 catalyst was fully comparable with that of the as-synthesized Tx-COF-2, as observed from PXRD, with a little de

Table 2. Substrate Tolerance Tests of Tx-COF-2 in Oxidative Hydroxylation of Arylboronic acids to Phenols[a]

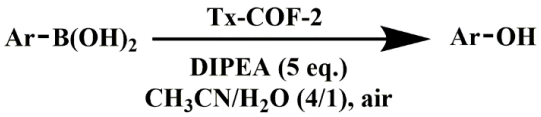

Entry	Ar	Time (h)	Yield[b] (%)
1	4-$HO_2CC_6H_4$	48	99
2	4-$CHOC_6H_4$	48	95
3	4-NO_2C6H_4	48	99
4	4-$H_3CO_2CC_6H_4$	48	92
5	4-CNC_6H_4	48	99
6	4-BrC_6H_4	48	87
7	C_6H_5	72	74

[a]Conditions: Arylboronic Acid (0.12 mmol), Tx-COF-2 (10 mg, 0.012 mmol), CH_3CN (1.6 mL), H_2O (0.4 mL), DIPEA (5.0 eq.), irradiation with 20 W white LEDs. [b]Yields of isolated products.

crease in the intensity[16] (Figure S11). Furthermore, after 10th catalytic run, Tx-COF-2 retained its microporous nature with a slight drop in the BET surface area, as shown by the N_2 adsorption-desorption isotherm (Figure 3b, Figure S12, Figure S13).

We then tested the versatility of the Tx-COF-2 as a photocatalyst for the conversion of different arylboronic acid derivatives to corresponding phenols. As shown in Table 2, Tx-COF-2, as a photocatalyst, can easily convert all the substituted arylboronic acids to the corresponding phenols. Usually, the reaction rate is faster with the substrates bearing electron-deficient groups (Table 2, entry 1-5) than that of the substrates bearing

electron-rich groups (Table 2, Entry 6-7). In reported literature, this selectivity has been explained according to the fact that the empty *p*-orbital of boron atoms present in the arylboronic acids having electron-withdrawing groups are more available for $O_2^{\bullet-}$ radical anion.[31]

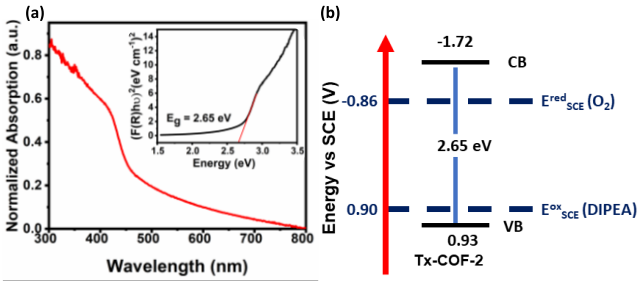

Figure 4. (a) UV-vis spectrum of Tx-COF-2 (Inset) Kubelka–Munk function plot to evaluate the bandgap of Tx-COF-2 and (b) Calculated position of the conduction band and valence band the of Tx-COF-2, the reduction potential of O_2, and oxidation potential of DIPEA.

To get more understanding about the photocatalytic process, various electronic properties of Tx-COF-2 were studied. Initially, the UV/vis absorption spectrum of Tx-COF-2 showed a broad absorption edge in the region from UV to visible light (Figure 4a). The optical band gap (E_g) of Tx-COF-2 was determined by Kubelka-Munk plot and estimated to be 2.65 eV, indicating its semiconducting nature (Figure 4a; inset). Cyclic voltammetry was further recorded to determine the oxidative potential of Tx-COF-2. CV experiment displayed an oxidation peak with an onset value of +0.93 V versus saturated calomel electrode (SCE), which corresponds to the valance band (VB) potential (E_{VB}) (Figure S9). The approximate conduction band (CB) potential (E_{CB}) was calculated using the equation, $E_{CB} = E_{VB} - E_g$. Thus, the E_{CB} value of Tx-COF-2 was estimated to be −1.72 V versus SCE. The reduction potential (E^{red}) of O2 is −0.86 V and the oxidation potential (E^{ox}) of DIPEA is +0.90 V (versus SCE). The photocatalysts having E_{VB} value greater than +0.90 V and E_{CB} value less than −0.86 V are expected to oxidize DIPEA which causes the reduction of O_2.[31] The E_{CB} and E_{VB} of Tx-COF-2 entirely meet the abovementioned criteria (Figure 4b). In addition, electron paramagnetic resonance (EPR) spectroscopy was carried out to confirm the generation of $O_2^{\bullet-}$ upon addition of the superoxide radical scavenger 5,5-dimethyl-1-pyrroline N-oxide (DMPO) (Figure S10). A probable reaction mechanism for the conversion is shown in Figure 5. Upon irradiation of visible light, the excited Intermediate of Tx-COF-2* was first generated, followed by an electron was extracted from DIPEA via a single-electron transfer (SET) process to generate a radical anion Tx-COF-2$^{\bullet-}$ which left a radical cation DIPEA$^{\bullet+}$. Then the Tx-COF-2$^{\bullet-}$ was oxidized by molecular O_2 to regenerate Tx-COF-2 for the upcoming cycle. Further, $O_2^{\bullet-}$ was filled to the vacant *p*-

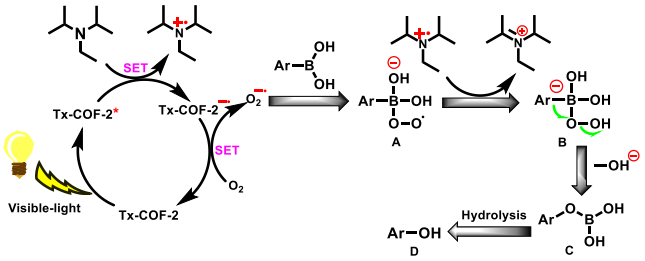

Figure 5. The probable reaction mechanism for the photocatalytic oxidative hydroxylation of arylboronic acids using Tx-COF-2 as the photocatalyst (SET: single-electron transfer).

orbital of boron, leading to the intermediate A. A hydrogen atom was extracted from DIPEA$^{\bullet+}$ to produce intermediate B. Next, loss of a $-OH^-$ ion and rearrangement formed intermediate C. Finally, intermediate C hydrolyzed to afford the desired phenolic product.

As mentioned earlier, the Tx-COF-2 was very stable in contact with 12 M HCl, which also caused a visual change of the color from yellowish to orange. This phenomenon encouraged us to investigate the sensing properties of Tx-COF-2 towards HCl. Upon exposure to HCl vapor, the suspension (0.5 mg mL^{-1} in 1,4-dioxane) of Tx-COF-2 went through a naked eye color change from light yellow to orange. When the HCl treated suspension was subjected to light at a wavelength of 365 nm, an orange fluorescence emission color was also observed (Figure 6a). This color change was completely reversible when HCl treated Tx-COF-2 exposed to the NH_3 vapor. The color changes occurred in fractions of a second, faster than those previously reported COF-based HCl sensors.[32] Notably, as-synthesized Tx-COF-2 was very weakly fluorescent, but HCl treated suspension of Tx-COF-2 showed remarkable enhancement in the fluorescence intensity. Thus, Tx-COF-2 could be used as a 'turn-on' sensor because it offered a high increment in the fluorescence intensity after treating with HCl vapor and reverted to its pristine weakly-fluorescent nature after exposure to NH_3 vapor. Besides, no degradation in the fluorescence intensity as well as in naked-eye color changes up to 10 alternating cycles of exposure to HCl and NH_3 vapor confirmed the excellent reversibility and structural rigidity of Tx-COF-2 as HCl sensor.

We then investigated the relationship between the fluorescent intensity of 1,4-Dioxane suspended Tx-COF-2 (0.5 mg mL^{-1}) and the concentration of HCl (diluted in 1,4-Dioxane). We observed that upon the addition of a small concentration of HCl (8 μmol L^{-1}) to Tx-COF-2 suspension, the weak-intensity peaks at 495 nm and 515 nm started disappearing, and a new peak appeared at 558 nm (λ_{ex}= 478 nm) (Figure 6b). The fluorescence intensity increased gradually upon increasing the concentration of HCl from 8 μmol L^{-1} to 63.5 μmol L^{-1} and remained unchanged after that. The lowest limit of detection was found to be 4.5 nmol L^{-1} from the calibration curve in the range of HCl concentration from 1 to 55 μmol L^{-1}, which showed linear correlation (R^2= 0.9864) with detection at 558 nm (Figure 6e). The fluorescence

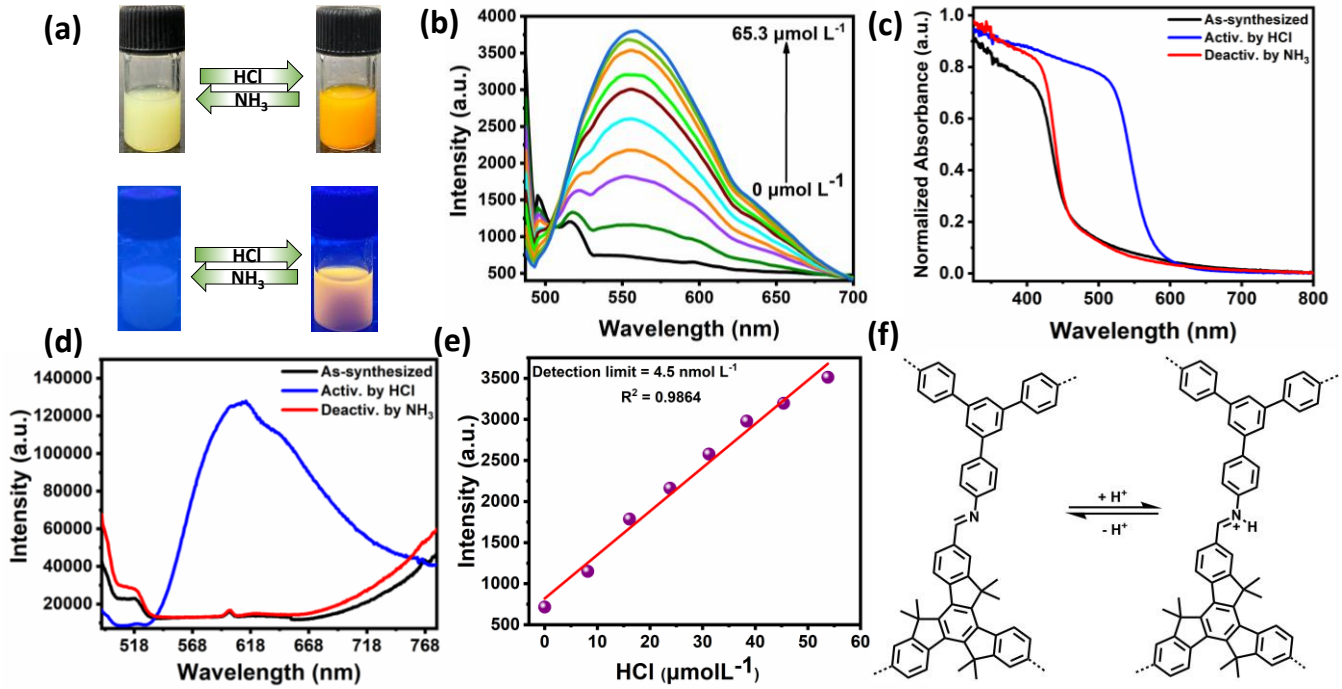

Figure 6. (a) Optical photograph of Tx-COF-2 suspension in 1,4-Dioxane after exposure to HCl and NH_3 vapor: Naked eye and in the UV-light (b) Fluorescence spectra of Tx-COF-2 suspension (0.5 mg mL^{-1}) in 1,4-Dioxane at λ_{ex}= 478 nm. (c) Solid-state UV-vis spectra of Tx-COF-2 after exposure to HCl and NH_3 vapor (d) Solid-state fluorescence spectra of Tx-COF-2 after exposure to HCl and NH_3 vapor (λ_{ex}=478 nm) (e) Calibration curve of fluorescence intensity versus HCl concentration and (f) Schematic representation of the protonation and deprotonation mechanism of the Tx-COF-2 after alternate exposure to HCl and NH_3 vapors.

lifetime decay of Tx-COF-2 was found to be 0.49 ns at 65.3 μmol L^{-1} HCl concentration (Figure S17). A possible mechanism of sensing toward HCl is shown in Figure 6f. The Tx-COF-2 presumably undergoes protonation at the imine nitrogen atom, which takes part in the conjugation of the COF and results in an apparent change in fluorescence emission as well as in color.[33] Previously reported COFs supports the fact of protonation at the nitrogen atom present in the COFs.[34] Next, the reusability and recyclability of Tx-COF-2 as HCl sensor were investigated and shown in Figure S15. Tx-COF-2 was recovered by the addition of a solution of triethylamine (1.6 mmol L^{-1}) from the HCl treated Tx-COF-2 at a concentration (1.6 mmol L^{-1}) until the pH = 7. Moreover, the selectivity of the Tx-COF-2 toward HCl was investigated by treating Tx-COF-2 suspension to the various acids at a concentration of 2.0 mmol L^{-1}. As shown in Figure S16, in comparison with the other acids, only HCl caused a significant enhancement in the fluorescence emission maxima of Tx-COF-2 when excited at 478 nm.

Next, we investigated the naked-eye detection of HCl vapor by Tx-COF-2 in a solid-state. A color change from yellow to orange was observed when Tx-COF-2 powder was exposed to HCl vapor and returned to its natural color after the exposure of NH_3 vapor (Figure S14 and Supplementary Video). In the UV-vis spectra, a red-shift in the absorbance maxima was observed after exposure to the HCl vapor and regenerated with NH_3 vapor (Figure 6c). In addition, when we recorded fluorescence spectra of Tx-COF-2 powder, fluorescence emission was observed for the HCl treated Tx-COF-2 powder and returned to as-synthesized non-fluorescent powder when exposed to NH_3 vapor (Figure 6d). In conclusion, these phenomena were observed presumably because of the protonation at the nitrogen center in the Schiff-base backbone of the Tx-COF-2.[35]

In summary, we have synthesized a novel dual-function Truxene-based COF using Schiff-base chemistry. Based on our results, Tx-COF-2 was found to be highly crystalline with permanent porosity and high chemical stability even in harsh chemical conditions for example 12 M HCl, 12 M NaOH, etc. Tx-COF-2 has been used for visible-light heterogeneous photocatalytic transformation of arylboronic acids to phenols with high efficiency. Most importantly, Tx-COF-2 has many advantages as a photocatalyst such as a reusability and insolubility in various organic solvents. Hence, we believe Tx-COF-2 could be a promising photocatalyst for chemical transformations. Besides, we tested Tx-COF-2 for HCl sensing and found very high sensitivity and selectivity toward HCl. We observed the 'turn-on' phenomenon in the fluorescence spectroscopy accompanied by naked eye color change in solid as well as in the dispersed state in rapid response time (<1 sec). Tx-COF-2 can sense HCl up to 4.5 nmol L^{-1}, which is the first example of very low detection for HCl sensing in COFs. This COF was found to be an excellent photocatalyst and sensor for HCl vapor. We believe that our work will open up several new strategies to develop simple and smart materials for practical applications, from naked eye readable sensors to photocatalysts.

ASSOCIATED CONTENT

Supporting Information.

This material is available free of charge via the Internet at http://pubs.acs.org."

Detailed synthetic procedure of monomers and Tx-COF-2, ^{1}H and ^{13}C NMR Spectra of substrates, FT-IR Spectra, SEM images, TGA curve, CV spectra, Fluorescence experiments and computational details of Tx-COF-2.

Crystallographic information files for Tx-COF-2 (AA, AB, SlipAA_X_0.5)

AUTHOR INFORMATION

Corresponding Author

Santanu Kumar Pal- Department of Chemical Sciences, Indian Institute of Science Education and Research (IISER) Mohali, Sector 81, Knowledge City, Manauli, 140306 (India), http://orcid.org/0000-0003-4101-4970
E-mail: skpal@iisermohali.ac.in, santanupal.20@gmail.com

Authors

Yogendra Nailwal- Department of Chemical Sciences, Indian Institute of Science Education and Research (IISER) Mohali, Sector 81, Knowledge City, Manauli, 140306 (India), https://orcid.org/0000-0003-3770-6464
Email: yogi.nails@gmail.com

A. D. Dinga Wonanke- School of Science and Technology, Nottingham Trent University, Clifton Lane, NG11 8NS, Nottingham, United Kingdom
Email: dinga.wonanke@ntu.ac.uk

Matthew A. Addicoat- School of Science and Technology, Nottingham Trent University, Clifton Lane, NG11 8NS, Nottingham, United Kingdom
Email: matthew.addicoat@ntu.ac.uk

Notes

The authors declare no competing financial interest.

ACKNOWLEDGMENT

M.A.A acknowledges HPC resources through Materials Chemistry Consortium EP/P020194. SKP acknowledges Project File No. CRG/2019/000901/OC from DST-SERB. We sincerely thank Dr. Adrene Freeda D'cruz for critical reading of the manuscript.

REFERENCES

(1) (a) Geng, K.; He, T.; Liu, R.; Dalapati, S.; Tan, K. T.; Li, Z.; Tao, S.; Gong, Y.; Jiang, Q.; Jiang, D. Covalent Organic Frameworks: Design, Synthesis, and Functions. *Chem. Rev*. **2020**, *120*, 8814–8933. (b) Chen, X.; Geng, K.; Liu, R.; Tan, K. T.; Gong, Y.; Li, Z.; Tao, S.; Jiang, Q.; Jiang, D. Covalent Organic Frameworks: Chemical Approaches to Designer Structures and Built-In Functions. *Angew. Chem., Int. Ed.* **2020**, *59*, 5050–5091. (c) Lohse, M. S.; Bein, T. Covalent Organic Frameworks: Structures, Synthesis, and Applications. *Adv. Funct. Mater*. **2018**, *28*, No. 1705553. (d) Huang, N.; Wang, P.; Jiang, D. Covalent Organic Frameworks: A Materials Platform for Structural and Functional Designs. *Nat. Rev. Mater*. **2016**, *1*, No. 16068. (e) Diercks, C. S.; Yaghi, O. M. The Atom, the Molecule, and the Covalent Organic Framework. *Science* **2017**, *355*, No. eaal1585. (f) Ding, S.-Y.; Wang, W. Covalent Organic Frameworks (COFs): from Design to Applications. *Chem. Soc. Rev*. **2013**, *42*, 548−568.

(2) (a) Waller, P. J.; Gándara, F.; Yaghi, O. M. Chemistry of Covalent Organic Frameworks. *Acc. Chem. Res*. **2015**, *48*, 3053−3063. (b) Kandambeth, S.; Dey, K.; Banerjee, R. Covalent Organic Frameworks: Chemistry beyond the Structure. *J. Am. Chem. Soc*. **2019**, *141*, 1807−1822. (c) Jin, Y.; Hu, Y.; Zhang, W. Tessellated multiparous two-dimensional covalent organic frameworks. *Nat. Rev. Chem*. **2017**, *1*, 0056−0067. (d) Evans, A. M.; Parent, L. R.; Flanders, N. C.; Bisbey, R. P.; Vitaku, E.; Kirschner, M. S.; Schaller, R. D.; Chen, L. X.; Gianneschi, N. C.; Dichtel, W. R. Seeded growth of single-crystal two-dimensional covalent organic frameworks. *Science* **2018**, *361*, 52−57.

(3) (a) Kalidindi, S. B.; Fischer, R. A. Covalent Organic Frameworks and Their Metal Nanoparticle Composites: Prospects for Hydrogen Storage. *Phys. Status Solidi B* **2013**, *250*, 1119−1127. (b) Zeng, Y.; Zao, R.; Zhao, Y. Covalent Organic Frameworks for CO_2 Capture. *Adv. Mater*. **2016**, *28*, 2855−2873. (c) Fan, H.; Mundstock, A.; Feldhoff, A.; Knebel, A.; Gu, J.; Meng, H.; Caro, J. Covalent Organic Framework−Covalent Organic Framework Bilayer Membranes for Highly Selective Gas Separation. *J. Am. Chem. Soc*. **2018**, *140*, 10094−10098.

(4) (a) Gao, Q.; Li, X.; Ning, G.-H.; Leng, K.; Tian, B.; Liu, C.; Tang, W.; Xu, H.-S.; Loh, K. P. Highly Photoluminescent Two-Dimensional Imine-Based Covalent Organic Frameworks for Chemical Sensing. *Chem. Commun*. **2018**, *54*, 2349−2352. (b) Ascherl, L.; Evans, E. W.; Hennemann, M.; Nuzzo, D. D.; Hufnagel, A. G.; Beetz, M.; Friend, R. H.; Clark, T.; Bein, T.; Auras, F. Solvatochromic Covalent Organic Frameworks. *Nat. Commun*. **2018**, *9*, No. 3802. (c) Rao, M. R.; Fang, Y.; Feyter, S. D.; Perepichka, D. F. Conjugated Covalent Organic Frameworks via Michael Addition−Elimination. *J. Am. Chem. Soc.* **2017**, *139*, 2421−2427. (d) Singh, H.; Devi, M.; Jena, N.; Iqbal, M. M.; Nailwal, Y.; Sarkar, A. D.; Pal, S. K. Proton-Triggered Fluorescence Switching in Self-Exfoliated Ionic Covalent Organic Nanosheets for Applications in Selective Detection of Anions. *ACS Appl. Mater. Interfaces*, **2020**, *12*, 13248-13255.

(5) (a) Sun, Q.; Aguila, B.; Earl, L. D.; Abney, C. W.; Wojtas, L.; Thallapally, P. K.; Ma, S. Covalent Organic Frameworks as a Decorating Platform for Utilization and Affinity Enhancement of Chelating Sites for Radionuclide Sequestration. *Adv. Mater*. **2018**, No. 1705479. (b) Mullangi, D.; Dhavale, V.; Shalini, S.; Nandi, S.; Collins, S.; Woo, T.; Kurungot, S.; Vaidhyanathan, R. Low-Overpotential Electrocatalytic Water Splitting with Noble-Metal-Free Nanoparticles Supported in a sp^3 N-Rich Flexible COF. *Adv. Energy Mater*. **2016**, *6*, No. 1600110. (c) Haldar, S.; Roy, K.; Nandi, S.; Chakraborty, D.; Puthusseri, D.; Gawli, Y.; Ogale, S.; Vaidhyanathan, R. High and Reversible Lithium-Ion Storage in Self-Exfoliated Triazole-Triformyl Phloroglucinol-Based Covalent Organic Nanosheets. *Adv. Energy Mater*. **2018**, *8*, No. 1702170. (d) Jin, S.; Supur, M.; Addicoat, M.; Furukawa, K.; Chen, L.; Nakamura, T.; Fukuzumi, S.; Irle, S.; Jiang, D. Creation of Super heterojunction Polymers via Direct Polycondensation: Segregated and Bicontinuous Donor−Acceptor π-Columnar Arrays in Covalent Organic Frameworks for Long-Lived Charge Separation. *J. Am. Chem. Soc*. **2015**, *137*, 7817−7827. (e) Xu, Q.; Dalapati, S.; Jiang, D. Charge Up in Wired Covalent Organic Frameworks. *ACS Cent. Sci*. **2016**, *2*, 586−587. (f) Banerjee, T.; Gottschling, K.; Savasci, G.; Ochsenfeld, C.; Lotsch, B. V. H2 Evolution with Covalent Organic Framework Photocatalysts. *ACS Energy Lett.* **2018**, *3*, 400−409. (g) Lv, J.; Tan, Y. X.; Xie, J.; Yang, R.; Yu, M.; Sun, S.; Li, M. D.; Yuan, D.; Wang, Y. Direct Solar-to-Electrochemical Energy Storage in a Functionalized Covalent Organic Framework. *Angew. Chem., Int. Ed*. **2018**, *57*, 12716−12720. (h) Luo, Z.; Liu, L.; Ning, J.; Lei, K.; Lu, Y.; Li, F.; Chen, J. A Microporous Covalent-Organic Framework with Abundant Accessible Carbonyl Groups for Lithium-Ion Batteries. *Angew. Chem., Int. Ed*. **2018**, *57*, 9443−9446. (i) Khayum, M. A.; Vijayakumar, V.; Karak, S.; Kandambeth, S.; Bhadra, M.; Suresh, K.; Acharambath, N.; Kurungot, S.; Banerjee, R. Convergent Covalent Organic Framework Thin Sheets as Flexible Supercapacitor Electrodes. *ACS Appl. Mater. Interfaces* **2018**, *10*, 28139−28146.

(6) (a) Meng, Z.; Aykanat, A.; Mirica, K. A. Proton Conduction in 2D Aza-Fused Covalent Organic Frameworks. *Chem. Mater*. **2019**, *31*, 819−825. (b) Ma, H.; Liu, B.; Li, B.; Zhang, L.; Li, Y.-G.; Tan, H.-Q.; Zang, H.-Y.; Zhu, G. Cationic Covalent Organic Frameworks: A Simple Platform of Anionic Exchange for Porosity Tuning and Proton Conduction. *J. Am. Chem. Soc*. **2016**, *138*, 5897−5903.

(7) (a) Crowe, J. W.; Baldwin, L. A.; McGrier, P. L. Luminescent Covalent Organic Frameworks Containing a Homogeneous and Heterogeneous Distribution of Dehydrobenzoannulene Vertex Units. *J. Am. Chem. Soc*. **2016**, *138*, 10120−10123. (b) Bhunia, A.; Esquivel, D.; Dey, S.; Fernández-Terán, R.; Goto, Y.; Inagaki, S.; Voort, P. V. D.; Janiak, C. A Photoluminescent Covalent Triazine Framework: CO_2 Adsorption, Light-Driven Hydrogen Evolution and Sensing of Nitroaromatics. *J. Mater. Chem. A* **2016**, *4*, 13450−13457. (c) Dalapati, S.; Jin, E.; Addicoat, M.; Heine, T.; Jiang, D. Highly Emissive Covalent Or-

ganic Frameworks. *J. Am. Chem. Soc*. **2016**, *138*, 5797−5800. (d) Haldar, S.; Chakraborty, D.; Roy, B.; Gangadhar, S. B.; Rinku, K.; Mullangi, D.; Hazra, P.; Kabra, D.; Vaidhyanathan, R. Anthracene-Resorcinol Derived Covalent Organic Framework as Flexible White Light Emitter. *J. Am. Chem. Soc*. **2018**, *140*, 13367−13374. (e) Das, P.; Mandal, S. K. A Dual-Functionalized, Luminescent and Highly Crystalline Covalent Organic Framework: Molecular Decoding Strategies for Vocs and Ultrafast TNP Sensing. *J. Mater. Chem. A* **2018**, *6*, 16246−16256.

(8) (a) Chen, G.-J.; Li, X.-B.; Zhao, C.-C.; Ma, H.-C.; Kan, J.-L.; Xin, Y.-B.; Chen, C.-X.; Dong, Y.-B. Ru Nanoparticles-Loaded Covalent Organic Framework for Solvent-Free One-Pot Tandem Reactions in Air. *Inorg. Chem.* **2018**, *57*, 2678−2685. (b) Shi, X.; Yao, Y.; Xu, Y.; Liu, K.; Zhu, G.; Chi, L.; Lu, G. Imparting Catalytic Activity to a Covalent Organic Framework Material by Nanoparticle Encapsulation. *ACS Appl. Mater. Interfaces* **2017**, *9*, 7481−7488. (c) Mu, M.; Wang, Y.; Qin, Y.; Yan, X.; Li, Y.; Chen, L. Two-Dimensional Imine-Linked Covalent Organic Frameworks as a Platform for Selective Oxidation of Olefins. *ACS Appl. Mater. Interfaces* **2017**, *9*, 22856−22863. (d) Han, Y.; Zhang, M.; Zhang, Y.-Q; Zhang, Z.-H. Copper Immobilized at a Covalent Organic Framework: An Efficient and Recyclable Heterogeneous Catalyst for the Chan−Lam Coupling Reaction of Aryl Boronic Acids and Amines. *Green Chem*. **2018**, *20*, 4891−4900. (e) Ding, S.-Y.; Gao, J.; Wang, Q.; Zhang, Y.; Song, W.-G.; Su, C.-Y.; Wang, W. Construction of Covalent Organic Framework for Catalysis: Pd/COF-LZU1 in Suzuki-Miyaura Coupling Reaction. *J. Am. Chem. Soc*. **2011**, *133*, 19816−19822. (f) Wang, X.; Han, X.; Zhang, J.; Wu, X.; Liu, Y.; Cui, Y. Homochiral 2D Porous Covalent Organic Frameworks for Heterogeneous Asymmetric Catalysis. *J. Am. Chem. Soc*. **2016**, *138*, 12332−12335. (g) Han, X.; Xia, Q.; Huang, J.; Liu, Y.; Tan, C.; Cui, Y. Chiral Covalent Organic Frameworks with High Chemical Stability for Heterogeneous Asymmetric Catalysis. *J. Am. Chem. Soc*. **2017**, *139*, 8693−8697. (h) Li, H.; Pan, Q.; Ma, Y.; Guan, X.; Xue, M.; Fang, Q.; Yan, Y.; Valtchev, V.; Qiu, S. Three-Dimensional Covalent Organic Frameworks with Dual Linkages for Bifunctional Cascade Catalysis. *J. Am. Chem. Soc*. **2016**, *138*, 14783−14788. (i) Lu, S.; Hu, Y.; Wan, S.; McCaffrey, R.; Jin, Y.; Gu, H.; Zhang, W. Synthesis of Ultrafine and Highly Dispersed Metal Nanoparticles Confined in a Thioether-Containing Covalent Organic Framework and Their Catalytic Applications. *J. Am. Chem. Soc*. **2017**, *139*, 17082−17088. (j) Mullangi, D.; Chakraborty, D.; Pradeep, A.; Koshti, V.; Vinod, C. P.; Panja, S.; Nair, S.; Vaidhyanathan, R. Highly Stable COF Supported $Co/Co(OH)_2$ Nanoparticles Heterogeneous Catalyst for Reduction of Nitrile/Nitro Compounds under Mild Conditions. *Small* **2018**, *14*, No. 1801233.

(9) Gámez-Valenzuela, S.; Echeverri, M.; Go´mez-Lor, B.; Martínez, J. I.; Delgado, M. C. R. In silico design of 2D polymers containing truxene-based platforms: insights into their structural and electronic properties. *J. Mater. Chem. C*, **2020**, *8*, 15416-15425.

(10) (a) Goubard, F.; Dumur, F. Truxene: A Promising Scaffold for Future Materials. *RSC Adv*. **2015**, *5*, 3521–3551. (b) Zhao, Q. Li, S.-H.; Chai, R.-L.; Ren, X.; Zhang, C. Two-Dimensional Conductive Metal–Organic Frameworks Based on Truxene. *ACS Appl. Mater. Interfaces* **2020**, *12*, 6, 7504-7509.

(11) (a) Battula, V. R.; Singh, H.; Kumar, S.; Bala, I.; Pal, S. K.; Kailasam, K. Natural Sunlight Driven Oxidative Homocoupling of Amines by a Truxene-Based Conjugated Microporous Polymer. *ACS Catal*. **2018**, *8*, 6751– 6759; b) Guadalupe, J.; Ray, A. M.; Maya, E. M.; Gómez-Lor, B.; Iglesias, M. Truxene-based porous polymers: from synthesis to catalytic activity. *Polym. Chem*. **2018**, *9*, 4585-4595. (c) Echeverri, M.; Gámez-Valenzuela, S.; González-Cano, R. C.; Guadalupe, J.; Cortijo-Campos, S.; Navarrete, J. T. L.; Iglesias, M.; Delgado, M. C. R.; Gómez-Lor, B. Effect of the Linkage Position on the Conjugation Length of Truxene-Based Porous Polymers: Implications for Their Sensing Performance of Nitroaromatics. *Chem. Mater*. **2019**, *31*, 6971–6978. (d) Valverde-González, A.; López Calixto, C. G.; Barawi, M.; Gomez-Mendoza, M.; de la Peña O'Shea, V. A.; Liras, M.; Gómez-Lor, B.; Iglesias, M. Understanding Charge Transfer Mechanism on Effective Truxene-Based Porous Polymers–TiO_2 Hybrid Photocatalysts for Hydrogen Evolution. *ACS Appl. Energy Mater*. **2020**, *3*, 4411-4420. (e) Liu, X.; Xu, Y.; Jiang, D. Conjugated Microporous Polymers as Molecular Sensing Devices: Microporous Architecture Enables Rapid Response and Enhances Sensitivity in Fluorescence-On and Fluorescence-Off Sensing. *J. Am. Chem. Soc*. **2012**, *134*, 8738– 8741. (f) Sadak, A. E.; Karakus-, E.; Chumakov, Y. M.; Dogan N. A.; Yavuz, C. T. Triazatruxene-Based Ordered Porous Polymer: High-Capacity CO_2, CH_4, and H_2 Capture, Heterogeneous Suzuki–Miyaura Catalytic Coupling, and Thermoelectric Properties. *ACS Appl. Energy Mater*., **2020**, *3*, 4983-4994. (g) Li, X. C.; Zhang, Y. Z.; Wang, C. Y.; Wan, Y.; Lai, W. Y.; Pang, H.; Huang, W. Redox-Active Triazatruxene-Based Conjugated Microporous Polymers for High-performance Supercapacitors. *Chem. Sci*. **2017**, *8*, 2959– 2965. (h) Bala, I.; Pal, S. K. Rod–disc oligomeric liquid crystal based on 4-cyanobiphenyl and truxene core. *Liq Cryst*. **2016**, *43*, 7, 963.

(12) (a) Fu, Q.; Bo, Z.-Y.; Ye, J.-H.; Ju, T.; Huang, H.; Liao, L.-L.; Yu, D.-G. Transition metal-free phosphonocarboxylation of alkenes with carbon dioxide via visible-light photoredox catalysis. *Nat. Commun.* **2019**, *10*, 3592. (b) Dauncey, E. M.; Dighe, S. U.; Douglas, J. J.; Leonori, D. A dual photoredox-nickel strategy for remote functionalization via iminyl radicals: radical ring-opening-arylation, -vinylation and -alkylation cascades. *Chem. Sci*. **2019**, *10*, 7728.

(13) (a) Pham, P. V.; Nagib, D. A.; MacMillan, D. W. C. Photoredox Catalysis: A Mild, Operationally Simple Approach to the Synthesis of a- Trifluoromethyl Carbonyl Compounds. *Angew. Chem., Int. Ed*. **2011**, *50*, 6119−6122. (b) Nguyen, J. D.; Tucker, J. W.; Konieczynska, M. D.; Stephenson, C. R. J. Intermolecular Atom Transfer Radical Addition to Olefins Mediated by Oxidative Quenching of Photoredox Catalysts. *J. Am. Chem. Soc*. **2011**, *133*, 4160−4163. (c) Nagib, D. A.; MacMillan, D. W. C. Trifluoromethylation of Arenes and Heteroarenes by Means of Photoredox Catalysis. *Nature* **2011**, *480*, 224−228. (d) Furst, L.; Narayanam, J. M. R.; Stephenson, C. R. Total Synthesis of (+)-Gliocladin C Enabled by Visible-Light Photoredox Catalysis. *Angew. Chem., Int. Ed.* **2011**, *50*, 9655−9659. (e) Yoon, T. P.; Ischay, M. A.; Du, J. Visible Light Photocatalysis as a Greener Approach to Photochemical Synthesis. *Nat. Chem*. **2010**, *2*, 527−532. (f) Tucker, J. W.; Nguyen, J. D.; Narayanam, J. M. R.; Krabbe, S. W.; Stephenson, C. R. J. Tin-free Radical Cyclization Reactions Initiated by Visible Light Photoredox Catalysis. *Chem. Commun*. **2010**, *46*, 4985−4987. (g) Du, J.; Yoon, T. P. Crossed Intermolecular [2 + 2] Cycloadditions of Acyclic Enones via Visible Light Photocatalysis. *J. Am. Chem. Soc*. **2009**, *131*, 14604−14605.

(14) (a) Marin, M. L.; Santos-Juanes, L.; Arques, A.; Amat, A. M.; Miranda, M. A. Organic Photocatalysts for the Oxidation of Pollutants and Model Compounds. *Chem. Rev*. **2012**, *112*, 1710−1750. (b) Neumann, M.; Fuldner, S.; Konig, B.; Zeitler, K. Metal-Free, Cooperative Asymmetric Organophotoredox Catalysis with Visible Light. *Angew. Chem., Int. Ed*. **2011**, *50*, 951−954. (c) Liu, H. J.; Feng, W.; Kee, C. W.; Zhao, Y. J.; Leow, D.; Pan, Y. H.; Tan, C. H. Organic Dye Photocatalyzed α-Oxyamination through Irradiation with Visible Light. Green Chem. **2010**, 12, 953−956. (d) Romero, N. A.; Nicewicz, D. A. Organic Photoredox Catalysis. *Chem. Rev*. **2016**, *116*, 10075−10166.

(15) Halder, A.; Kandambeth, S.; Biswal, B. P.; Kaur, G.; Roy, N. C.; Addicoat, M.; Salunke, J. K.; Banerjee, S.; Vanka, K.; Heine, T.; Verma, S.; Banerjee, R. Decoding the Morphological Diversity in Two Dimensional Crystalline Porous Polymers by Core Planarity Modulation. *Angew. Chem., Int. Ed*. **2016**, *55*, 7806–7810.

(16) (a) Wei, P.; Qi, M.; Wang, Z.; Ding, S.; Yu, W.; Liu, Q.; Wang, L.; Wang, H.; An, W.; Wang, W. Benzoxazole-Linked Ultrastable Covalent Organic Frameworks for Photocatalysis. *J. Am. Chem. Soc.* **2018**, *140*, 4623–4631. (b) Yan, X.; Liu, H.; Li, Y.; Chen, W.; Zhang, T.; Zhao, Z.; Xing, G.; Chen, L. Ultrastable Covalent Organic Frameworks via Self-Polycondensation of an A_2B_2 Monomer for Heterogeneous Photocatalysis. *Macromolecules* **2019**, *52*, 7977– 7983.

(17) (a) Burton, G. W.; Doba, T.; Gabe, E.; Hughes, L.; Lee, F. L.; Prasad, L.; Ingold, K. U. Autoxidation of Biological Molecules. 4. Maximizing the Antioxidant Activity of Phenols. *J. Am. Chem. Soc.*

1985, *107*, 7053−7065. (b) Greenberg, M.; Dodds, M.; Tian, M. Naturally Occurring Phenolic Antibacterial Compounds Show Effectiveness against Oral Bacteria by a Quantitative Structure−Activity Relationship Study. *J. Agric. Food Chem*. **2008**, *56*, 11151−11156. (c) Quideau, S.; Deffieux, D.; Douat-Casassus, C.; Pouysegu, L. Plant Polyphenols: Chemical Properties, Biological Activities, and Synthesis. *Angew. Chem., Int. Ed*. **2011**, *50*, 586−621.

(18) Zou, Y.-Q.; Chen, J.-R.; Liu, X.-P.; Lu, L.-Q.; Davis, R. L.; Jørgensen, K. A.; Xiao, W.-J. Highly Efficient Aerobic Oxidative Hydroxylation of Arylboronic Acids: Photoredox Catalysis Using Visible Light. *Angew. Chem., Int. Ed.* **2012**, *51*, 784-788.

(19) Pitre, S. P.; McTiernan, C. D.; Ismaili, H.; Scaiano, J. C. Mechanistic insights and kinetic analysis for the oxidative hydroxylation of arylboronic acids by visible light photoredox catalysis: a metal-free alternative. *J. Am. Chem. Soc*. **2013**, *135*, 13286–13289.

(20) Prier, C. K.; Rankic, D. A.; MacMillan, D. W. C. Visible Light Photoredox Catalysis with Transition Metal Complexes: Applications in Organic Synthesis. *Chem. Rev*. **2013**, *113*, 5322–5363.

(21) (a) Graetzel, M. Artificial Photosynthesis: Water Cleavage into Hydrogen and Oxygen by Visible Light. *Acc. Chem. Res*. **1981**, *14*, 376–384. (b) Meyer, T. J. Chemical Approaches to Artificial Photosynthesis. *Acc. Chem. Res*. **1989**, *22*, 163–170.

(22) Takeda, H.; Ishitani, O. Development of Efficient Photocatalytic Systems for CO_2 Reduction using Mononuclear and Multinuclear Metal Complexes Based on Mechanistic Studies. *Coord. Chem. Rev.* **2010**, *254*, 346–354.

(23) (a) Lowry, M. S.; Bernhard, S. Synthetically Tailored Excited States: Phosphorescent, Cyclometalated Iridium (III) Complexes and their Applications. *Chem. - Eur. J.* **2006**, 12, 7970– 7977; b) Ulbricht, C.; Beyer, B.; Friebe, C.; Winter, A.; Schubert, U. S. Recent Developments in the Application of Phosphorescent Iridium (III) Complex Systems. *Adv. Mater*. **2009**, *21*, 4418–4441.

(24) (a) Lalevée, J.; Blanchard, N.; Tehfe, M.-A.; Morlet-Savary, F.; Fouassier, J. P. Green Bulb Light Source Induced Epoxy Cationic Polymerization under Air using Tris(2,20 -bipyridine)ruthenium(II) and Silyl Radicals. *Macromolecules* **2010**, *43*, 10191– 10195. (b) Lalevée, J.; Peter, M.; Dumur, F.; Gigmes, D.; Blanchard, N.; Tehfe, M.-A.; Morlet-Savary, F.; Fouassier, J. P. Subtle Ligand Effects in Oxidative Photocatalysis with Iridium Complexes: Application to Photopolymerization. *Chem. - Eur. J.* **2011**, *17*, 15027– 15031. (c) Fors, B. P.; Hawker, C. J. Control of a Living Radical Polymerization of Methacrylates by Light. *Angew. Chem., Int. Ed*. **2012**, *51*, 8850–8853.

(25) Howerton, B. S.; Heidary, D. K.; Glazer, E. C. Strained Ruthenium Complexes are Potent Light-Activated Anticancer Agents. *J. Am. Chem. Soc*. **2012**, *134*, 8324–8327.

(26) Nicewicz, D. A.; MacMillan, D. W. C. Merging Photoredox Catalysis with Organocatalysis: The Direct Asymmetric Alkylation of Aldehydes. *Science* **2008**, *322*, 77–80.

(27) Ischay, M. A.; Anzovino, M. E.; Du, J.; Yoon, T. P. Efficient Visible Light Photocatalysis of [2+2] Enone Cycloadditions. *J. Am. Chem. Soc*. **2008**, *130*, 12886–12887.

(28) Narayanam, J. M. R.; Tucker, J. W.; Stephenson, C. R. J. Electron-Transfer Photoredox Catalysis: Development of a Tin-Free Reductive Dehalogenation Reaction. *J. Am. Chem. Soc*. **2009**, *131*, 8756–8757.

(29) Bi, S.; Thiruvengadam, P.; Wei, S.; Zhang, W.; Zhang, F.; Gao, L.; Xu, J.; Wu, D.; Chen, J.-S.; Zhang, F. Vinylene-bridged two-dimensional covalent organic frameworks via knoevenagel condensation of tricyanomesitylene. *J. Am. Chem. Soc*. **2020**, *142*, 11893–11900.

(30) (a) Wagay S. A.; Rather, I. A.; Ali, R. Functionalized Truxene Scaffold: A Promising Advanced Organic Material for Digital Era, *ChemistrySelect*, **2019**, *4*, 12272-12288. (b) Dai, P.; Dong, H.; Liang, M.; Cheng, H.; Sun, Z.; Xue, S. Understanding the Role of Electron Donor in Truxene Dye Sensitized Solar Cells with Cobalt Electrolytes. *ACS Sustainable Chem. Eng*. **2017**, *5*, 97–104. (c) Shi, K.; Wang, J.-Y.; Pei, J. π-Conjugated aromatics based on truxene: Synthesis, self-assembly, and applications. *Chem. Rec*. **2015**, *15*, 52–72.

(31) Johnson, J. A.; Luo, J.; Zhang, X.; Chen, Y.-S.; Morton, M. D.; Echeverría, E.; Torres, F. E.; Zhang, J. Porphyrin-metalation-mediated tuning of photoredox catalytic Properties in metal-organic frameworks. *ACS Catal*. **2015**, *5*, 5283–5291.

(32) (a) EL-Mahdy, A. F. M.; Elewa, A. M.; Huang, S.-W.; Chou, H.-H.; Kuo, S.-W. Dual-Function Fluorescent Covalent Organic Frameworks: HCl Sensing and Photocatalytic H_2 Evolution from Water. *Adv. Opt. Mater*., **2020**, 2000641. (b) El-Mahdy, A. F. M.; Lai, M.-Y.; Kuo, S.-W. A Highly Fluorescent Covalent Organic Framework as a Hydrogen Chloride Sensor: Roles of Schiff Base Bonding and Pi-stacking. *J. Mater. Chem. C* **2020**, *8*, 9520–9528.

(33) Cui, F.-Z.; Xie, J.-J.; Jiang, S.-Y.; Gan, S.-X.; Ma, D.-L.; Liang, R.-R.; Jiang, G.-F.; Zhao, X. A Gaseous Hydrogen Chloride Chemosensor Based on a 2D Covalent Organic Framework. *Chem. Commun*. **2019**, *55*, 4550–4553.

(34) Ascherl, L.; Evans, E. W.; Gorman, J.; Orsborne, S.; Bessinger, D.; Bein, T.; Friend, R. H.; Auras, F. Perylene-Based Covalent Organic Frameworks for Acid Vapor Sensing. *J. Am. Chem. Soc*. **2019**, *141*, 15693–15699.

(35) Kulkarni, R.; Noda, Y.; Barange, D. K.; Kochergin, Y. S.; Lyu, P.; Balcarova, B.; Nachtigall, P.; Bojdys, M. J. Real-Time Optical and Electronic Sensing with a Beta-Amino Enone Linked, Triazine-Containing 2D Covalent Organic Framework. *Nat. Commun*. **2019**, *10*, 3228.

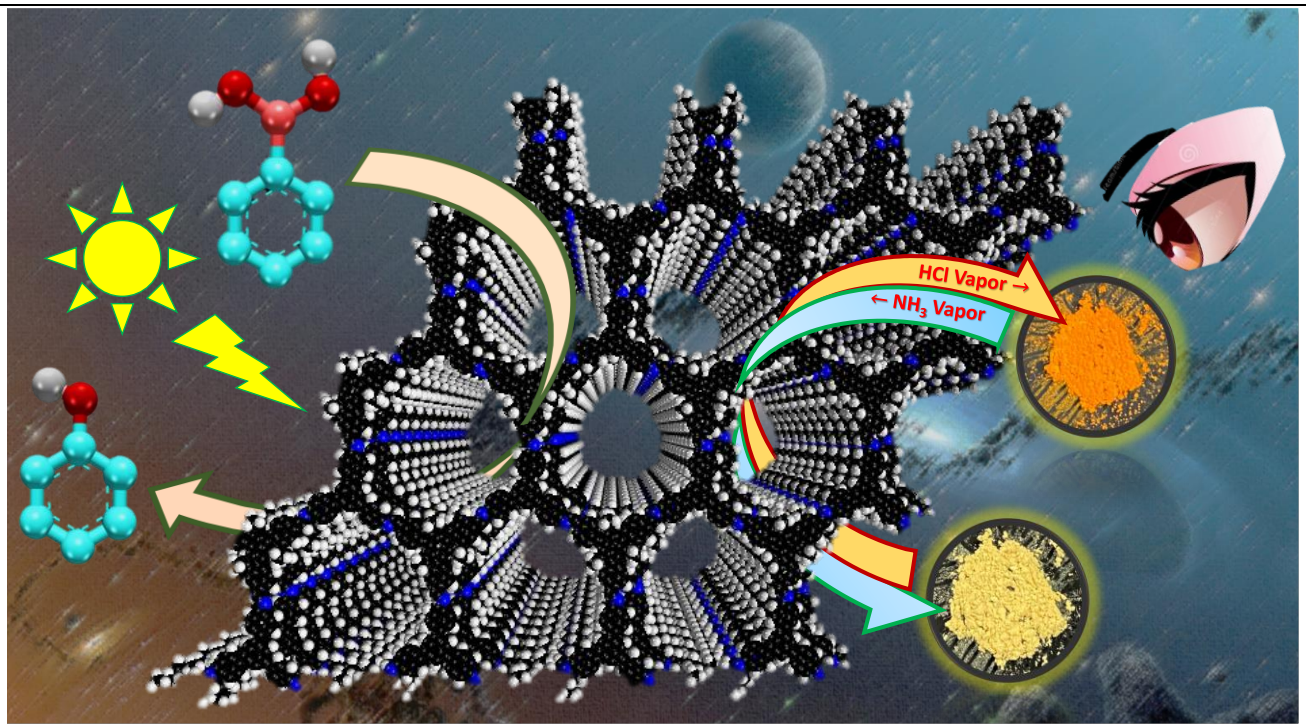

Insert Table of Contents artwork here